International Journal of Infrared and Millimeter Waves, Vol. 2, No. 4, 1981

MILLIMETER-WAVE ABSORPTION MEASUREMENTS IN LOW-LOSS DIELECTRICS USING AN UNTUNED CAVITY RESONATOR

Friedrich Kremer and Jerald R. Izatt*

Max-Planck Institute für Festkorperforschung
7000 Stuttgart 80, Fed. Rep. Germany

Received March 13, 1981

Millimeter wave absorption measurements are usually complicated by scattering from the sample and by standing waves resulting from internal reflections. These problems can be largely overcome by using an untuned cavity resonator. The dielectric properties of the sample are determined from a measurement of the change in cavity Q produced by introduction of the sample into the cavity. For lamellar samples, Maxwell's equations can be used to find an explicit relationship between the change in cavity Q and the samples complex refractive index. Several measuring techniques based on the use of lamellar samples are presented, and their characteristics are illustrated both analytically and by laboratory measurements at 70 GHz on PTFE, polyethylene and plexiglas.

Key words: millimeter wave spectroscopy, untuned cavity resonator, dielectric losses.

*On leave from Département de Physique et Laboratoire de recherche en optique et laser, Université Laval, Québec, Qué., Canada, G1K 7P4

0195-9271/81/0700-0675$03.00/0

I. Introduction

Untuned cavity resonators have long been used for the measurement of microwave absorption spectra of gaseous samples(1,2). Their utility as long pathlength, high throughput absorption cells for use in far infrared spectroscopy has also been demonstrated(3). Recently it has been shown that such cavities can also be employed to measure small dielectric losses in solid materials(4,5). This technique can be used to circumvent many difficulties usually associated with surface reflections, standing waves, scattering and diffraction when measurements are made on such samples in the 30 to 1000 GHz region.

When monochromatic radiation is fed into an appropriately designed, high-Q, untuned cavity a very large number of cavity modes is excited and the resulting field is highly homogeneous and isotropic. Measurement of the decrease in Q resulting from introduction of a sample into the cavity is a very sensitive method of determining the dielectric losses in the sample. Since any radiation scattered or reflected by the sample is returned to the cavity field the measured loss in entirely due to absorption. However, deduction of the absorption coefficient α from such a measurement requires an accurate estimate of the effective absorption path inside the sample. This obviously depends, in principle, both on the sample geometry and on its refractive index n. The latter determines both the direction of propagation inside the sample and the nature of the reflections at its surfaces.

Llewellyn-Jones et al.(5) have used an untuned cavity resonator to measure the absorption coefficient of several low loss polymeric materials at 156 GHz. Their results demonstrated that for bulk samples with dimensions of the order of ten wavelengths or more the absorption coefficients were only weakly dependent on sample geometry. They established an empirical factor which was used to correct for the effect of reflection at the sample boundaries. The dependence of this correction factor on the sample's refractive index was weak enough under their experimental conditions so that accurate knowledge of n was not required in order to determine α with acceptable accuracy. To pursue further the investigation of the ultimate accuracy and the conditions of

applicability of untuned cavity measurements, we have studied one particular sample geometry in greater theoretical and experimental detail. By using parallel-faced lamellar samples it is possible to employ an analytic solution to the boundary value problem at the sample surfaces to relate the sample's complex refractive index to the measured change in cavity Q. The effect of n on the accuracy with which α can be determined can then be evaluated in a straightforward way. Assessment of the relative importance of other experimental parameters is also facilitated.

This work constitutes part of a detailed analysis of the performance of a large untuned cavity resonator which has been constructed in our laboratory for use in the 40 to 170 GHz region. Among the applications planned for this cavity is the measurement of biological samples, and it has already been used to make preliminary measurements of the temperature dependence of the absorption at 53 GHz in green algae, yeast and E. Coli near the freezing point of water(6).

II. Theory

In this section elements of the basic theory of the untuned microwave resonator, which was developed originally by Lamb(1), will be reviewed. The scheme for calculating the sample absorption coefficient from the measured change in Q will be described, and refinements of the basic procedure based on the use of a calibration sample and on the intercomparison of multiple samples will be presented.

A. Lamb's hole method

It is convenient to associate a quality factor Q with each of the principal cavity loss mechanisms. The Q-factor is defined generically by the following relationship:

$$Q^{-1} = \frac{\text{rate of loss of photons from cavity}}{\omega \cdot \text{number of photons stored in cavity}} . \qquad (1)$$

Here ω is the angular frequency of the radiation in the cavity. The Q-factor associated with absorption in the sample, which it will be convenient to denote by

Q_S, can be evaluated by comparing the absorption loss to the loss of photons through a hole of known size that can be opened in the cavity wall. The Q-factor associated with the hole will be denoted by Q_H. It is also useful to associate a factor Q_R with the remaining resonator losses such as absorption in the walls and losses through the aperture that is used to feed radiation into the cavity.

In practice the radiation field inside the cavity is sampled by one or more detectors which produce signals proportional to the photon density. It is therefore convenient to employ rate equations formulated explicitly in terms of the number of photons in the cavity. The latter is constructed with dimensions of the order of 100 times the wavelengths at which measurements are to be made. As a consequence the cavity modes are very closely spaced in frequency, and when radiation from a narrow-band source is fed into the cavity many modes are excited at essentially equal rates. In addition, the whole ensemble of cavity modes can be continuously shifted back and forth in space by use of a mechanical mode stirrer whose period is small compared to the integration time of the detector system. Under these conditions the radiation field is highly homogeneous and isotropic throughout the cavity. The photon density, averaged over the detector integration time and all of the excited modes, therefore has the constant value N/Ω, where N is the total number of photons and Ω is the cavity volume.

If the cavity contains an absorbing sample and the calibration hole is open, a source feeding radiation into the cavity at an average rate M will establish a stationary photon population N which satisfies the following equation.

$$\frac{dN}{dt} = 0 = M - \ell_R N - \ell_H N - \ell_S N \qquad (2)$$

Here the loss coefficients ℓ_R, ℓ_H and ℓ_S correspond respectively to photon losses inherent in the cavity structure, losses through the calibration hole, and absorption in the sample. Each of the loss rates, $\ell_R N$, $\ell_H N$ and $\ell_S N$, can also be expressed in the form $\ell N = \omega N/Q$. The addition of the individual loss rates in eq. 2 to obtain the total cavity loss rate is then seen to correspond to addition of the reciprocals of the corresponding

Q-factors and produces the reciprocal of the total cavity Q.

In order to determine ℓ_S, measurements corresponding to the following set of conditions are made while the source power is held constant.

i) calibration hole closed, no sample

$$M = \ell_R N_O \tag{3}$$

ii) calibration hole open, no sample

$$M = \ell_R N_H + \ell_H N_H \tag{4}$$

iii) calibration hole closed, sample in cavity

$$M = \ell_R N_S + \ell_S N_S \tag{5}$$

If the linear range of the detection system is not exceeded, the signal measured at each step of the procedure is proportional to the corresponding value of N. The necessity of evaluating the detector responsivity can be avoided by employing only ratios of detector signals measured under the various cavity conditions. Let $R_H = N_H/N_O$ and $R_S = N_S/N_O \cdot R_H$ and R_S are then equal to the ratios of the corresponding detector signals, and simultaneous solution of eqs. 3-5 yields the following expressions for ℓ_S and ℓ_R.

$$\ell_S = \frac{R_H}{R_S} \left(\frac{1 - R_S}{1 - R_H} \right) \ell_H. \tag{6}$$

$$\ell_R = \left(\frac{R_H}{1 - R_H} \right) \ell_H \tag{7}$$

By considering the cavity radiation field as a photon gas and calculating the rate at which photons escape through the hole, Lamb (1) derives an expression for Q_H, which is equivalent to

$$\ell_H = \frac{cA_H}{4\Omega}. \tag{8}$$

Here c is the speed of light and A_H is the area of the calibration hole. Diffraction effects, which are neglected in Lamb's derivation, may reduce the efflux of photons through the hole. The measurements to be pre-

sented in Section III indicate that hole edge effects can be quite large.

B. Calculation of Absorption Coefficient

To calculate the number of photons per second which strike the hole Lamb reckons the number of photons approaching the hole at a given incidence angle Θ, and this quantity is then integrated over a complete hemisphere. To about the same level of approximation, the number of photons which strike a thin flat sample at a given incidence angle can be obtained by simply multiplying Lamb's corresponding expression by two; i.e., whereas the hole is single sided as seen from the cavity, photons strike the sample with equal probability from both sides. When diffraction is neglected the transmission of photons through the hole displays no angular dependence other than that arising from the varying aspect angle it presents to photons arriving at various angles. On the other hand, even neglecting edge effects, the absorbing sample has angle-dependent reflection and transmission coefficients. These coefficients are also functions of the wavelength λ, the sample thickness d, and the dielectric constants of the sample.

It is convenient to express the dielectric properties of the sample in terms of the complex index of refraction $\tilde{n} = n + ik$. The real part n is just the refractive index of Snell's law, and the absorption coefficient in Lambert's law is related to k by $\alpha = 2\omega k/c$. The sample reflection coefficient, which specifies the fraction of the radiation incident at angle Θ that is reflected from the sample back into the cavity field, will be denoted by $R = R(\Theta,n,k,d,\lambda)$. The transmission coefficient, which is defined in analogous fashion, will be denoted by $T = T(\Theta,n,k,d,\lambda)$. These quantities are indicated in Figure 1. Both coefficients are also polarization dependent, and polarizations normal and parallel to the plane of incidence will be denoted respectively by subscripts σ and π. The fraction A of the photons striking the sample that is absorbed is given in terms of R and T by the energy conservation relationship, $R + T + A = 1$. Since the radiation field in the cavity is unpolarized, the total absorption coefficient for the lamellar sample is obtained by averaging over the two perpendicular polari-

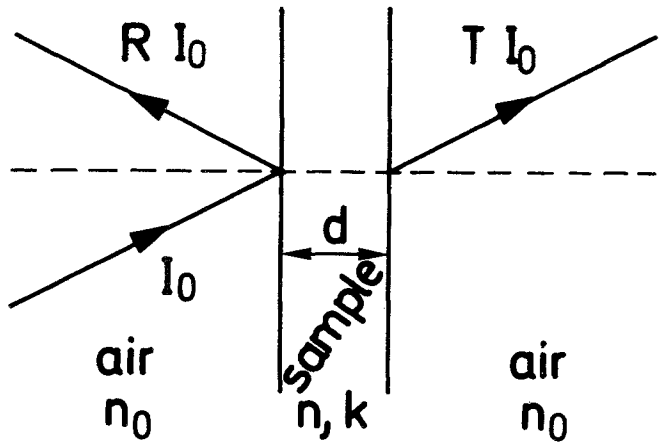

Fig. 1. Sample geometry.

zation components. Incorporation of these considerations into Lamb's derivation yields

$$\ell_S N_S = \frac{A_S c N_S}{\Omega} \int_0^{\pi/2} A_T(\theta,n,k,d,\lambda)\, \sin\theta\cos\theta d\theta \qquad (9)$$

Here $A_T = (A_\sigma + A_\pi)/2$, and A_S is the area of each side of the sample.

Finally, combination of eqs. 6,8 and 9 yields

$$I(n,k,d,\lambda) = \int_0^{\pi/2} A_T(\theta,n,k,d,\lambda)\sin\theta\cos\theta d\theta = \frac{A_H}{4A_S}\frac{R_H}{R_S}\left(\frac{1-R_S}{1-R_H}\right) \qquad (10)$$

Hadley and Dennison(7) have solved the Maxwell-equation boundary-value problem for the case of a parallel-sided sheet of absorbing material sandwiched between two infinite, lossless dielectrics. For the present case

where the space on both sides of the lamella is occupied by air, their formulae for R and T can be reduced to the following form.

For radiation polarized normal to the plane of incidence:

$$R_\sigma = (A \cosh\gamma - B \cos\alpha)/D_\sigma$$

$$T_\sigma = 8\rho_{s\sigma}^2/p_o^2 D_\sigma$$

$$A_\sigma = 1 - R_\sigma - T_\sigma$$

$$D_\sigma = C \cosh\gamma + D \sinh\gamma + E \cos\alpha + S \sin\alpha$$

$$\gamma = 4\pi q_{s\sigma} d/\lambda \qquad (11)$$

$$\alpha = 4\pi p_{s\sigma} d/\lambda$$

$$q_{s\sigma} = \frac{1}{\sqrt{2}} \{[(n^2-k^2-\sin^2\theta)^2 + 4n^2k^2]^{1/2} - (n^2-k^2-\sin^2\theta)\}^{1/2}$$

$$p_{s\sigma} = \frac{1}{\sqrt{2}} \{[(n^2-k^2-\sin^2\theta)^2 + 4n^2k^2]^{1/2} + (n^2-k^2-\sin^2\theta)\}^{1/2}$$

$$p_{s\sigma}^2 = q_{s\sigma}^2 + p_{s\sigma}^2$$

$$p_o = n_o \cos\theta$$

$$A = [(\rho_{s\sigma}^2 + p_o^2)^2 - 4p_{s\sigma}^2 p_o^2]/p_o^4$$

$$B = [(\rho_{s\sigma}^2 - p_o^2)^2 + 4q_{s\sigma}^2 p_o^2]/p_o^4$$

$$C = [(\rho_{s\sigma}^2 + p_o^2)^2 + 4p_{s\sigma}^2 p_o^2]/p_o^4$$

$$D = 4p_{s\sigma}(\rho_{s\sigma}^2 + p_o^2)/p_o^3$$

$$E = -[(\rho_{s\sigma}^2 - p_o^2) - 4q_{s\sigma}^2 p_o^2]/p_o^4$$

$$F = 4q_{s\sigma}(\rho_{s\sigma}^2 - p_o^2)/p_o^3$$

The reflection and transmission coefficients for parallel polarization have the same form as R_σ and T_σ, and can be obtained as follows. Leave γ and α unchanged. In the formula for T_σ and in the formulae for the constants A through F: $q_{s\sigma}$ is replaced by

$$q_{s\pi} = [q_{s\sigma}(n^2-k^2)-2p_{s\sigma}nk] / (n^2+k^2)^2;$$ $p_{s\sigma}$ is replaced by

$$p_{s\pi} = p_{s\sigma}(n^2-k^2)+2q_{s\sigma}nk / (n^2+k^2)^2;$$ and $p^2_{s\sigma}$ is replaced by

$$p^2_{s\pi} = q^2_{s\pi} + p^2_{s\pi}.$$

Some sample curves calculated using these formulae are shown in Fig. 2. The integral on the right side of eq. 9 has been evaluated numerically for the same values on n, k and λ, and is shown as a function of d in Fig. 3. In spite of the angle averaging, interference effects are clearly evident in Fig. 3. Note also that interference effects can be seen in the reflection and transmission factors of Fig. 2.

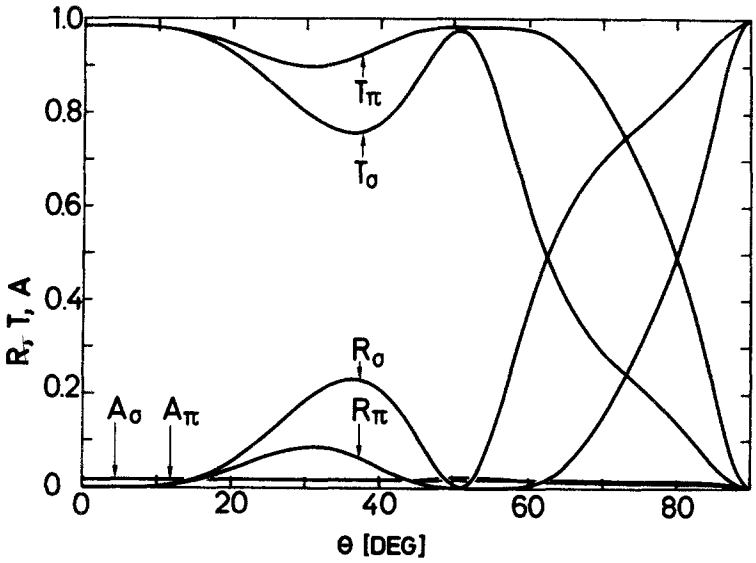

Fig. 2. Reflection, transmission and absorption factors for a lamellar sample with $n_o = 1$, $n = 1.5$, $k = 0.0005$ cm^{-1}, $d = 1$ cm and $\nu = 70$ GHz.

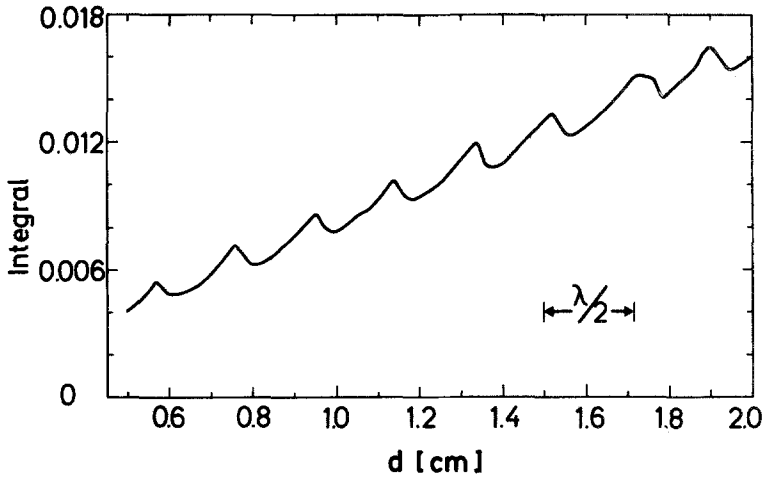

Fig. 3. The absorption integral of eq. 9 plotted as a function of sample thickness for a lamellar sample with $n_o = 1$, $n = 1.5$, $k = 0.0005$ cm^{-1} and $\nu = 70$ GHz.

If the detector signal ratios specified in eq. 10 are measured for given λ and d, then n and k remain the only unknown quantities. Simple numerical techniques can be employed to evaluate the integral and determine the locus of points in n, k space which satisfy this equation. k can then be determined if n is known. If n is only approximately known, the accuracy of the corresponding estimation of k is determined by the structure of the locus in n, k space.

C. Use of a calibration sample

As an alternative to the hole method, an absorbing sample with known dielectric properties can be used to calibrate the measurements. The theoretical loss rate associated with a lamellar calibration sample can be calculated from eq. 9. It is convenient to denote this loss rate by ℓ_C and also to use the subscript C to identify

all other quantities associated with the calibration sample. For example, the experimental loss rates for the unknown sample and for the resonator, can be obtained from eqs. 6 and 7 by replacing ℓ_H and R_H by ℓ_C and R_C respectively.

D. Comparison of multiple samples

In some circumstances it is unnecessary to use an idependently determined loss for calibration purposes. The dielectric properties of an unknown sample can be obtained directly from comparison of two or more pieces of the sample material identical in every respect except for their thickness. If two such samples are identified by subscripts 1 and 2 and the corresponding detector signal ratios with respect to the empty cavity are called R_{S1} and R_{S2}, then application of eqs. 3,5 and 10 to each of the samples in turn leads to the following equation.

$$\frac{I_1(n,k,d_1,\lambda)}{I_2(n,k,d_2,\lambda)} = \frac{R_{S2}}{R_{S1}} \left(\frac{1-R_{S1}}{1-R_{S2}}\right) \qquad (12)$$

Here again, by numerical evaluation of the integrals, I_1 and I_2, the locus of points in n, k space which are consistent with the measured detector ratios can be found. The values of ratios corresponding to additional sample thicknesses can also be determined experimentally, and each of them defines a curve in n, k space. For strongly absorbing samples the intersection of three or more such curves can be used to determine n and k simultaneously(8). When absorption in the sample is very weak the curves cross one another at too shallow an angle for this procedure to be used. However, this same circumstance makes it possible to obtain a good estimate of k when n is only approximately known.

A second class of intersample comparisons can also be useful; i.e., the comparison of lamellar samples of the same thickness but different surface area. Let the area of the larger sample, denoted as sample 3, be β times as great as that of the first, so that $\ell_{S3} = \beta\ell_{S1}$. Denote the ratio of the detector signal measured with the larger sample to that measured with the smaller sample by R_{31}. Application of eq. 5 to both samples

then leads directly to the following result

$$\frac{\beta R_{31}-1}{1-R_{31}} = \frac{\ell_R}{\ell_{S1}} \qquad (13)$$

Because of this relationship, which we have also verified experimentally, the quantity on the left remains constant for comparisons between sample 1 and all other samples of the same thickness, regardless of their surface area. This relationship can also be derived without postulating explicitly that $\ell_{S3} = \beta\ell_{S1}$, but the derivation is too long to be reproduced here. The usefulness of eq. 13 is related to the way in which errors in the measurement of the detector ratios are propagated when eq. 12 is used to calculate I_1/I_2 from experimental measurements.

E. Error analysis

Consider the two measurement sequences symbolized in Fig. 4. In the first sequence samples 1 and 2, which have

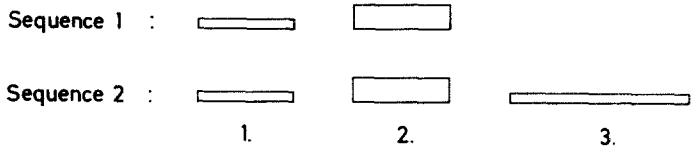

Fig. 4. Measurement sequences used to illustrate the added accuracy which can be achieved by comparing samples of different surface area.

the same sample area but different thickness are compared. This is the situation represented by eq. 12, and it will be convenient to denote the ratio I_1/I_2 determined in this way by $W = \frac{R_{S2}}{R_{S1}} \left(\frac{1-R_{S1}}{1-R_S^2}\right)$. Recall that the detector ratios R_{S1} and R_{S2} result from comparison of the respective samples with the empty cavity.

In measurement sequence 2, three samples are compared to one another in pairs. Samples 1 and 2 bear the same relationship to one another as before. Sample 3 has the same thickness as sample 1 but a surface area β times as large. Let the ratio of the detector signal measured with sample 2 in the cavity to that measured with sample 1 in the cavity be denoted by R_{21}. Similarly R_{31} is the detector signal ratio for samples 3 and 1. By applying eq. 5 to each of the samples in succession and then invoking eq. 13 the ratio I_1/I_2 can also be expressed as follows.

$$W = \frac{I_1}{I_2} = \frac{R_{21}(1-R_{31})}{(\beta R_{31}-1)(1-R_{21}) + (1-R_{31})} \tag{14}$$

If, it is now assumed that the sample thickness and β are perfectly known and also that the percentage error in the measurement of each of the detector ratios has the same value, $\Delta R/R$, then a straight-forward error propagation calculation shows that the percentage error in W can be written as follows for each of the measurement sequences. In both cases

$$\frac{\Delta W}{W} = (G^2+H^2)^{1/2} \frac{\Delta R}{R} \tag{15}$$

For sequence 1,

$$G = \frac{1+V}{V}, \quad H = \frac{1+VW}{VW} \tag{16}$$

For sequence 2, G is unchanged but

$$H = \frac{(W-1)(1+\beta VM)}{VW(\beta-1)} \tag{17}$$

The factor V in eqs. 16 and 17 is the ratio of the rate of loss in sample 2 to that inherent in the resonator; i.e., $V = \ell_{S2}/\ell_R$. Note also that $W = \ell_{S1}/\ell_{S2}$, and that $\ell_{S3}/\ell_R = \beta VW$. In order to avoid undue perturbation of the field in the cavity we have assumed that neither ℓ_{S2}/ℓ_R nor ℓ_{S3}/ℓ_R should exceed unity. Under these conditions G has a minimum value of 2, but achieving this value with a low-loss dielectric sample requires that the resonator losses be extremely small. W and hence H, can vary over a considerable range depending on the sample parameters and the comparison sequence that is employed; i.e., hole method, standard sample, multiple sample, etc.. Some representative plots which show the potential advantage of the three-sample sequence corresponding to eq. 14 are shown in Fig. 5. Note that a large value of β can usually be achieved experimentally only for relatively strong absorbers. For a weak absorber, the initial sample diameter must be relatively large in order to produce a measurable signal, and a large increase in sample diameter is then precluded by the finite dimensions of the cavity resonator.

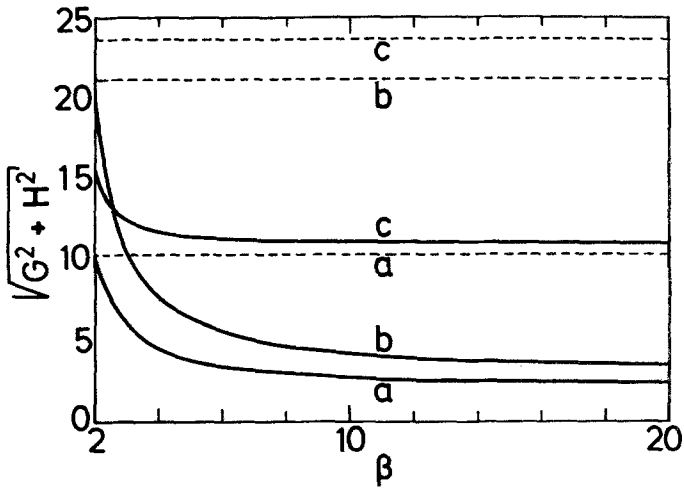

Fig. 5. Error reduction resulting from use of sample sequence 2. Dashed lines correspond to sequence 1 and solid lines to sequence 2. a) V = 1, W = 0.1; b) V = 0.5, W = 0.1; c) V = 0.1, W = 0.5.

III. Experiment

A. Description

The overal experimental system is shown schematically in Fig. 6. The untuned cavity resonator is a cylinder 40 cm in diameter and 80 cm long. It has highly reflecting gold-plated walls with textured inner surfaces, and a mode stirrer, which rotates at about 15 Hz. The mm-wave power is radiated from a horn inside the resonator, which is directed at an off-center point on the mode stirrer. The input power is measured by crystal detector 1. A small fraction of the field intensity inside the resonator is coupled out with a horn and measured by a second crystal detector 2. Both detector signals are amplified and averaged with a time constant, which is long compared to the period of the mode stirrer, in order to integrate over the modes of the resonator. To correct for power variations in the source, the signal of detector 2 is divided by that of detector 1. Backward-wave oscillators are used as mm-wave sources (Siemens RWO 60, RWO 80, RWO 110). An extra loop is employed to control the output-level and frequency.

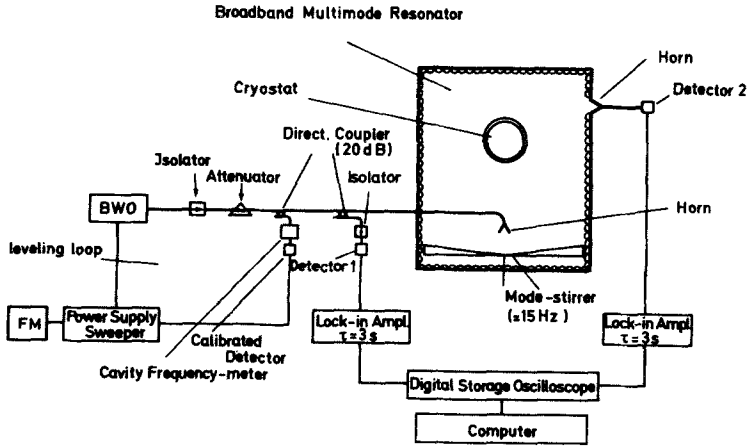

Fig. 6. Schematic diagram of the untuned resonator set-up.

The degree of isotropy and homogeneity of the radiation inside the resonator has been measured in two different ways: i) Changing the polarization of the out-coupling horn and also moving it to different positions does not alter the time-averaged, normalized detector signal by more than ±1.5%. ii) Changing the position of the sample inside the resonator changes the detector signal by less than ±0.5%. The same variability is observed when the two detectors are compared directly to one another. Thus the measurement uncertainties associated with cavity imperfections and incomplete mode stirring are comparable to the detector errors, and the overal reproductibility of the measurements is about ±1%.

The resonator has 60 mm diameter openings at six different positions. Each of them has a flange 30 mm long which is capped at the outermost extremity. One of these is used as the calibration hole when Lamb's procedure is employed.

B. Measurements

Measurements were made with disc-shaped samples of PTFE, polyethylene and plexiglas. In order to improve the approximation to the lamellar configuration used in the calculations, the edges of the discs were covered with aluminium foil. For each material, measurements were made by the hole method, by the use of a standard calibration sample, and by intercomparison of samples of different thickness.

The standard calibration sample was a fused silica disc (Schott Suprasil I), 80 mm in diameter and 4.98 mm in thickness. For this sample $n = 1.96 \pm 0.01$ and $k = (8.12 \pm 0.01) \times 10^{-4}$ cm^{-1} at 56.7 GHz. Measurements with this sample yield a value of $\sim 2 \times 10^5$ for the Q of our untuned resonator cavity.

Since more than one sample thickness was available for each material, the hole and standard sample methods were repeated for each thickness. Note that eqs. 15 and 16 can be used to estimate the error associated with these methods simply by replacing ℓ_{S2} by either ℓ_H or ℓ_C in the definitions of V and W. This procedure establishes confidence limits on the experimental determination of the right hand side of either eq. 10 or eq. 12. Numeri-

cal evaluation of the appropriate integral(s) then defines a region in n, k space for each value of the sample thickness d, and the experimental results for the samples of different thickness are self-consistent only for the n, k domain where these regions overlap.

The results for plexiglas are shown in Fig. 7. Note that in this case the standard sample method yields an absorption coefficient that is only very weakly dependent on n, whereas the two-sample comparisons yield little information on k but greatly restrict the range of possible n values. The two sets of date are mutually consistent only for the narrow range of n and k values that is shaded black. The hole method measurements show an intermediate sensitivity to n and k, but produce k values which are inconsistent with the results of the other two methods. We attribute this discrepancy to the complex structure of the calibration hole, which apparently presents an effective area for photon escape which is only ~ 40% of its geometric area.

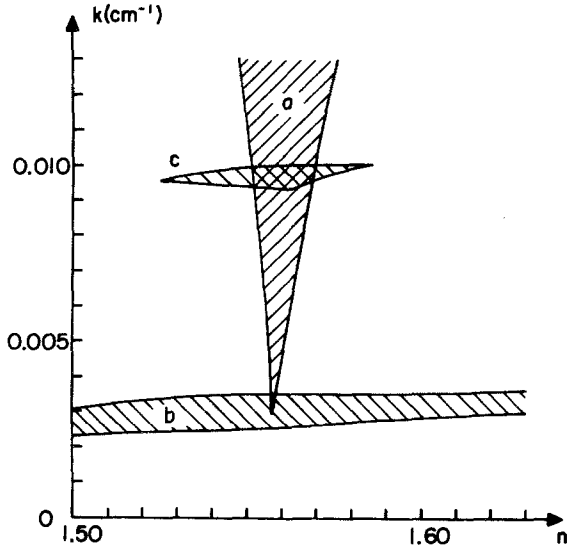

Fig. 7. Regions in n, k space determined by applying each of the three measuring techniques to plexiglas at 70 GHz, a) comparison of multiple samples of plexiglas of different thickness; b) comparison with a standard Suprasil sample; c) hole method.

For the weaker absorbers, PTFE and polyethylene, the comparison of samples of different thickness served only to fix an upper limit on k. The standard sample method produced a much more tightly defined value, which once again is very insensitive to n. The results are given in Table I.

TABLE I. Experimental results for PTFE, polyethylene and plexiglas at 70 GHz.

Sample	Area [cm^2]	Thickness [mm]	n	k ($10^{-4} cm^{-1}$)
PTFE	153.56	1.82 3.75 7.92	1.38*	2.1 ± 0.2
Polyethylene	153.56	1.99 3.94 7.99	1.46*	1.9 ± 0.2
Plexiglas	78.16	1.75 3.69 7.67	1.56	32 ± 3

* Values extrapolated from far-infrared measurements (10,11).

IV. Conclusion

We have demonstrated several techniques for measuring the imaginary part of the complex index of refraction of low-loss dielectrics. Used in concert they can also yield the value of n for absorbers of intermediate strength, such as plexiglas. The requirement to use an estimated value of n in the case of very weak absorbers is rendered less objectionable by the very weak dependence of k on n in these substances. For scattering samples like powders the methods presented here appear to be the best yet proposed for dielectric measurements in the mm- and submm-wave regime.

Because of the weak absorption of the materials considered here it was necessary to use samples of relatively large surface area for the measurements. As a consequence, use of the three-sample sequence illustrated in Fig. 4 was not attempted. It can easily be calculated, for example, that even in the case of plexiglas the use of a disc large enough to fill the entire cross-sectional area of our cavity resonator would reduce $\Delta W/W$ only by a factor of 3. When measurements are to be made on strong absorbers much greater increases in precision can be achieved by this means(8).

Acknowledgements

We wish to thank Professor Ludwig Genzel for many stimulating discussions of various aspects of millimeter wave dielectric measurements, Mr. D. Böhme and Mr. W. Schlieter for expert technical assistance with the measurements. Furthermore we thank Mr. M. Lemke (Philips Research Laboratory, Hamburg) for measuring the standard calibration sample.

References

1. W.E. Lamb, Jr., Phys. Rev. 70, 308 (1946).

2. G.E. Becker and S.H. Autler, Phys. Rev. 70, 300 (1946).

3. H.A. Gebbie and R.A. Bohlander, Appl. Optics 11, 723 (1972).

4. H.A. Willis, W. Reddish, K.A. Buckingham, D.T. Llewellyn-Jones, R.J. Knight and H.A. Gebbie, Polymer 22, 20 (1981).

5. D.T. Llewellyn-Jones, R.J. Knight, P.H. Moffat and H.A. Gebbie, IEE Proc-A 127 (8), 535 (1980).

6. F. Kremer, L. Genzel and F. Drissler, Proceedings of the International Symposium on Electromagnetic Waves and Biology, Paris, 1980.

7. L.N. Hadley and D.M. Dennison, J. Opt. Soc. Am. 37, 451 (1947).

8. J.R. Izatt and F. Kremer, to be published in Appl. Optics.

9. K.K. Mon and A.J. Sievers, Appl. Optics 14, 1054 (1975).

10. J.E. Chamberlain and H.A. Gebbie, Appl. Optics 5, 393 (1966).

11. G.W. Chantry, J.W. Fleming, P.M. Smith, M. Cudby and H.A. Willis, Chem. Phys. Lett. 10, 473 (1971).